

Phase transition of asymmetric diblock copolymer induced by nanorods of different properties

Yu-Qi Guo(郭宇琦)

Citation: Chin. Phys. B, 2021, 30 (**4**): 048301. DOI: 10.1088/1674-1056/abcf3c
Journal homepage: http://cpb.iphy.ac.cn; http://iopscience.iop.org/cpb

What follows is a list of articles you may be interested in

Enhanced hyperthermia performance in hard-soft magnetic mixed $Zn_{0.5}Co_xFe_{2.5-x}O_4/SiO_2$ composite magnetic nanoparticles

Xiang Yu(俞翔, Li-Chen Wang(王利晨, Zheng-Rui Li(李峥睿, Yan Mi(米岩), Di-An Wu(吴迪安), and Shu-Li He(贺淑莉)

Chin. Phys. B, 2021, 30 (**3**): 036201. DOI: 10.1088/1674-1056/abc67c

Enhancement in solar hydrogen generation efficiency using InGaN photoelectrode after surface roughening treatment with nano-sized Ni mask

Tao Tao, Zhi Ting, Li Ming-Xue, Xie Zi-Li, Zhang Rong, Liu Bin, Li Yi, Zhuang Zhe, Zhang Guo-Gang, Jiang Fu-Long, Chen Peng, Zheng You-Dou

Chin. Phys. B, 2014, 23 (**9**): 096203. DOI: 10.1088/1674-1056/23/9/096203

Effect of shear on the symmetric diblock copolymer/nanorod mixture: A dissipative particle dynamics study

He Lin-Li, Zhang Rui-Fen, Ji Yong-Yun

Chin. Phys. B, 2012, 21 (**8**): 088301. DOI: 10.1088/1674-1056/21/8/088301

Phase transition of asymmetric diblock copolymer induced by nanorods of different properties*

Yu-Qi Guo(郭宇琦)†

Department of Chemistry and Chemical Engineering, Lvliang University, Lishi 033000, *China*

(Received 7 August 2020; revised manuscript received 12 November 2020; accepted manuscript online 1 December 2020)

We investigate the microphase transition of asymmetric diblock copolymer induced by nanorods of different properties using cell dynamics simulation and Brown dynamics. The results show the phase diagram and representative nanostructures of the diblock copolymer nanocomposite. Various structures such as sea-island structure (SI), sea-island and lamellar structure (SI-L), and lamellar structure (L) are observed in the phase diagram. The system undergoes phase transition from SI-L to SI or from L to SI with increasing length of A-like sites for all numbers of nanorods except 10 and 300, and from SI to L with increasing number of nanorods for all lengths of A-like sites. Notably, the polymer system transforms from a tilted layered structure to a parallel lamellar, perpendicular lamellar, and subsequently sea-island structure with increasing length of A-like sites for a rod number of 240. To gain more detailed insight into these structural formation mechanisms, we analyze the evolution kinetics of the system with various lengths of A-like sites of the rods. The pattern evolution and domain growth of the ordered parallel/perpendicular lamellar structure are also investigated. Furthermore, the effects of the wetting strength, rod-rod interaction, polymerization degree, and length of nanorods on the self-assembled structure of asymmetric diblock copolymer/nanorods are studied. Our simulations provide theoretical guidance on the construction of complex-assembled structures and the design of novel functional materials.

Keywords: self-assemble, block copolymer, nanorods, phase transition

PACS: 83.10Tv, 83.80.Tc, 62.23.St, 64.75.Jk **DOI:** 10.1088/1674-1056/abcf3c

1. Introduction

The development of nanotechnology has progressed significantly in resent decades, and substantial effort has been devoted to research of unique structural, mechanical, electrical, optical, magnetic, and barrier properties of nanoparticles. However, the control of the distribution of nanoparticles within multi-component polymeric blends and their assembled structures remains highly challenging. One of the new and developing methods to regulate the assembled architectures of nanoparticles is to coat particles with different chemistries. In other words, these nanoparticles contain two compartments of different chemical compositions or surface properties within each particle, i.e., Janus nanoparticles. Owing to their asymmetrical surface properties, Janus nanoparticles are promising candidates for applications in the construction of complex-assembled structures and the design of novel functional materials. Nevertheless, beyond the coating of nanoparticles, particle shape is another important factor affecting the functionalities and potential applications of polymer-matrix composites. A number of approaches have been developed to control the spatial organization and assembly structures of spherical nanoparticles; however, hierarchical assemblies of nanorods with anisotropic shape, especially Janus nanorods, have rarely been investigated.

Balazs *et al.* investigated the assembled structure of nanoscale rods and binary blend. Their simulations demonstrated that when low-volume fractions of nanoscale rods were immersed in a binary phase-separating blend, they self-assembled into needle-like, percolating networks; however increasing the rod concentration beyond the effective percolation threshold caused the system to self-assemble into a lamellar morphology, with layers of wetted rods alternating with layers of the majority component fluid.[1] Ma *et al.* found that the rod-rod interaction and preferential adsorption of one of two immiscible phases on mobile rods caused the system to self-assemble into a droplet-like structure in a symmetric binary mixture containing mobile nanoscale rods.[2] Researchers have begun investigating the simplest polymers, which have exhibited ordered structures on the nanometer scale and, astonishingly, electrical and structural integrity.

Subsequently, Ma *et al.* investigated the phase behavior of nanoscale rods in diblock copolymer scaffolds, and developed a novel and simple approach to control and design the ordering of nanowire structures.[3] Subsequently, a series of relevant studies have been conducted using different methods.[4–20] Liang *et al.* investigated mixtures of symmetric diblock copolymers/rigid nanorods,[4] cylindrical diblock copolymers/rigid nanorods[5] and mixtures of diblock copolymers and mono- or bidisperse nanorods[6] via dissipative par-

*Project supported by the Scientific and Technological Innovation Programs of Higher Education Institutions in Shanxi (Grant No. 2019L0957), the Key Research and Development Project of the Introduction of High-Level Scientific and Technological Talents in Lvliang (Grant No. 201701102), and the Shanxi Provincial Natural Science Foundation, China (Grant No. 201801D221109).

†Corresponding author. E-mail: guoyuqi1988@sina.cn

© 2021 Chinese Physical Society and IOP Publishing Ltd

ticle dynamics (DPD) simulation. This method has also been used to investigate the structure and dynamics of the self-assembly of bundles formed by nanorods of different flexibilities in the gyroid phase of the diblock copolymer matrix,[7] as well as to study the mechanism by which the nanorod surface properties regulate the compatibilization behavior and morphology transition in demixing polymer blends.[8] Ma *et al.* used the self-consistent field theory to investigate the self-assembly of hard rod-shaped particles with an affinity for block A in diblock AB copolymer templates. They controlled the nanometer-length-scale structures by changing the particle concentration and volume fraction of block A.[9] Yan *et al.* simulated the self-assembly of nanorods in phase-separating A:B:C ternary melts,[10] as well as A- and B-coated rods in an AB phase-separating blend,[11] using a coarse-grained approach that combines a Cahn–Hilliard (CH) model for a polymer blend with Brownian dynamics (BD) simulation for the rods. Meanwhile, coarse-grained molecular dynamic simulation has been performed to investigate nanorod-filled polymer nanocomposites.[12–14] Langevin field theoretic simulation is a useful approach to study the distribution of nanorods in diblock copolymer thin films.[15] Osipov *et al.* studied the orientation ordering and spatial distribution of nanorods[16] as well as nanorods of various lengths[17] in the lamellae phase of diblock copolymers using both molecular statistical theory and DPD simulations.

Relevant experimental studies have also been conducted.[21–34] Russell *et al.*[21] investigated the assembly of surface-functionalized CdSe nanorods in polystyrene-*b*-poly(methyl methacrylate) (PS-*b*-PMMA) thin films. Their methodology enabled the assembly of the nanorods into templates and caused the sequestration of those nanorods into defined regions of a patterned surface, which is important when considering the electronic and photoactive applications of such a nanorod type. Additionally, Shenhar *et al.*[22] investigated the co-assembly of PS-*b*-PMMA and CdSe nanorods in ultrathin films. They considered the effects of copolymer size and nanorod filling fraction, and found that the combination of short nanorods and/or short copolymers was more prone to morphological defects, whereas assembling long nanorods with long copolymers resulted in highly organized nanorod morphologies. A few researchers have studied the assembly of gold nanorods/PS-*b*-PMMA,[23] gold nanorods/poly(styrene-*b*-2-vinylpyridine) (PS-*b*-P2VP),[24] and CdSe nanorods/poly(styrene-*b*-4-vinylpyridine) (PS-*b*-P4VP).[25,26] Moreover, Lai *et al.*[27] presented a facile strategy for the directed self-assembly of gold nanorods (AuNRs) in patterned PS-*b*-PMMA thin films, and found that an ordered AuNR assembly in a block copolymer pattern can be achieved at high surface coverage, although the surface coverage depends on the aspect ratio of the nanorods; furthermore, larger nanorods align in the channels more readily but accumulate at slightly lower densities.

Recently, nanorods with different properties, especially Janus nanorods, have been developed widely owing to the progress in nanotechnology. The self-assembly of Janus cylinders into hierarchical superstructures was observed by Walther *et al.*,[35] who presented detailed studies regarding the interfacial self-assembly of slightly amphiphilic Janus cylinders.[36] Subsequently, Yan *et al.* investigated the directed self-assembly of Janus nanorods in binary polymer mixtures.[37] Schweizer *et al.* investigated the real and Fourier space structure and phase behaviors of compositionally symmetric AB Janus rods using microscopic integral equation theory.[38] Recently, the diffusion of Janus rod-shaped nanoparticles in a dense Lennard–Jones fluid was studied using molecular dynamics simulations.[39]

Additionally, in a previous work we investigated the phase transition of a symmetric diblock copolymer induced by nanorods of different surface chemistries.[40]

Here, we investigate the phase transition of an asymmetric diblock copolymer induced by nanorods of different properties using a hybrid computational model. In Section 2, we describe the computational methodologies employed in this study. The results and relevant discussions are presented in Section 3, and the conclusions are provided in Section 4.

2. Model and method

To explore the phase behavior of the mobile nanorods in an asymmetric diblock copolymer, we use a hybrid method referred to as the CH/BD model, which has been widely used by various researchers.[41–45] The diblock copolymer is composed of A and B components, and the degrees of polymerization of blocks A and B are N_{A} and N_{B}, respectively. Herein, the diblock copolymer is treated as asymmetric, i.e., $N_{\mathrm{A}} \neq N_{\mathrm{B}}$. In the model, the phase separation of the asymmetric diblock copolymer is described through a CH model and the motion of the nanorods (including transition and rotation) is decided by a BD simulation.

The CH model[46–49] has been referenced in a number of studies.[50–59] In the cell dynamics method, an appropriate order parameter is discretized on a lattice, taking the value $\psi(i,t)$ in each cell i at time t. A suitable choice for an asymmetric diblock copolymer is the compositional order parameter $\psi(\boldsymbol{r}) = \phi_{\mathrm{A}}(\boldsymbol{r}) - \phi_{\mathrm{B}}(\boldsymbol{r}) + (1-2f)$, where ϕ_{A} and ϕ_{B} are local volume fractions of blocks A and B, respectively; f is the fraction of A monomers in the diblock, $f = N_{\mathrm{A}}/(N_{\mathrm{A}}+N_{\mathrm{B}})$; and $\boldsymbol{r}$ is the spatial position of each component. The flux of ψ is proportional to the local gradient of the chemical potential, which in turn is proportional to the derivative of the free energy F with respect to the order parameter,

$$\partial\psi/\partial t = \Gamma\nabla^2(\delta F\psi/\delta\psi), \tag{1}$$

where Γ is the mobility of the order parameter.

The rigid rods are described by discrete entities; each nanorod has a center-of-mass position $\boldsymbol{r}_i$ and an orientation angle θ_i measured from a fixed direction. The variables $\boldsymbol{r}_i$ and θ_i for the ith rod obey the following Langevin equations:

$$\begin{aligned} \partial \boldsymbol{r}_i/\mathrm{d}t &= -M_1 \partial F/\partial \boldsymbol{r}_i + \eta_i, \\ \partial \theta_{\mathrm{i}}/\mathrm{d}t &= -M_2 \partial F/\partial \theta_{\mathrm{i}} + \xi_i, \end{aligned} \tag{2}$$

where M_1 and M_2 represent the "motion" and "rotation" mobility coefficients, and η_i and ξ_i are thermal fluctuations that satisfy the fluctuation-dissipation relations. Equations (1) and (2) are discretized and numerically integrated on a 64×64 square lattice, which has periodic boundary conditions in both x and y directions.

The free energy F consists of three parts: $F = F_{\mathrm{GL}} + F_{\mathrm{CPL}} + F_{\mathrm{RR}}$. The diblock copolymer is described by the first term, F_{GL}, which is the Ginzburg–Landau free energy

$$\begin{aligned} F_{\mathrm{GL}} = {} & \frac{\alpha}{2} \iint \mathrm{d}\boldsymbol{r}\mathrm{d}\boldsymbol{r}' G(\boldsymbol{r},\boldsymbol{r}')[\psi(\boldsymbol{r}) - \psi_0][\psi(\boldsymbol{r}') - \psi_0] \\ & + \iint \mathrm{d}\boldsymbol{r} \left[w(\psi) + \frac{D}{2} (\nabla \psi(\boldsymbol{r}))^2 \right], \end{aligned} \tag{3}$$

where the first term corresponds to the long-range part. It is a relatively simple expression, in which $G(\boldsymbol{r},\boldsymbol{r}')$ is Green's function defined by the equation $-\nabla^2 G(\boldsymbol{r},\boldsymbol{r}') = \delta(\boldsymbol{r} - \boldsymbol{r}')$. Here α is an important parameter that describes the strength of the long-range force owing to the covalent linkage between the A and B components and determines the thickness of the domains.[63,64] The next term corresponds to the short-range part. Therein, $w(\psi) = [-\frac{a}{2} + \frac{b}{2}(1-2f)^2]\psi(\boldsymbol{r})^2 + \frac{v}{3}(1-2f)\psi(\boldsymbol{r})^3 + \frac{u}{4}\psi(\boldsymbol{r})^4$,[63,64] where a is related to the depth from the order-disorder transition temperature, and the coefficients b, v, and u are phenomenological parameters. $D(\nabla\psi(\boldsymbol{r}))^2$ represents the free energy cost for spatial composition inhomogeneity and thus is related to the interfacial regions. D is also a constant and scales with the Kuhn statistical segment length.

For the interaction between the rods and diblock copolymer, we take

$$F_{\mathrm{CPL}} = \int \mathrm{d}\boldsymbol{r}_i \sum_i \int \mathrm{d}\boldsymbol{s}_i V(\boldsymbol{r} - \boldsymbol{s}_i)(\psi(\boldsymbol{r}) - \psi_w)^2, \tag{4}$$

where $\boldsymbol{s}_i = \boldsymbol{r}_i + \delta\boldsymbol{s}_i$ ($\delta\boldsymbol{s}_i = 1$) represents a point on the surface of the ith nanorod, and $\int \mathrm{d}\boldsymbol{r}_i$ represents the integral over the length of the ith nanorod. By setting $\psi_w = 1$ and $\psi_w = -1$, we model the phase A-like and phase B-like surface sites of a nanorod. When ψ_w is set to 1 and -1, it indicates that the rod is energetically favored in phases A and B, respectively. We take the short-range wetting interaction $V(\boldsymbol{r} - \boldsymbol{s}_i) = V_0 \exp(-|\boldsymbol{r} - \boldsymbol{s}_i|/r_0)$, where $V_0(>0)$ is a wetting strength parameter that refers to the interaction strength between the diblock copolymer and rods; r_0 indicates the range of the interaction, and is also tunable by varying the chemical nature and length of the chains coated on the rods.

The rod-rod interaction F_{RR} is taken to be purely repulsive. This term is dependent on the distance and angle between pairs of rods i and j

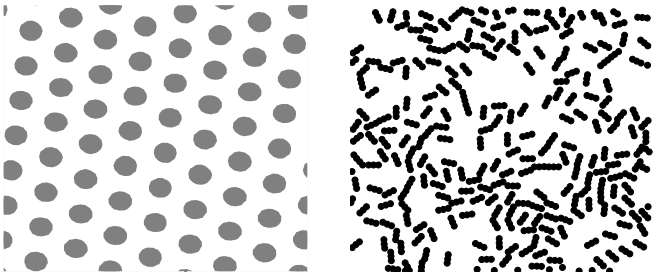
$$F_{\mathrm{RR}} = \begin{cases} \chi \sum_i \sum_j (L - |\boldsymbol{r}_i - \boldsymbol{r}_j|^2) \left[\dfrac{4}{3} - \cos^2(\theta_i - \theta_j) \right], & \text{for } |\boldsymbol{r}_i - \boldsymbol{r}_j| < L \\ 0, & \text{for } |\boldsymbol{r}_i - \boldsymbol{r}_j| \geq L. \end{cases} \tag{5}$$

Here the constant χ characterizes the strength of the interaction between rods and L is the rod length. La denotes the length of A-like sites of the rod.

In our simulation, the initial distribution of ψ is specified by random uniform distributions in the range $[-0.01, 0.01]$, and N rigid rods of length L are randomly dispersed in the asymmetric diblock copolymer; the motion of the rods is not restricted to lattice sites. We set the parameters as $A = 1.3$, $\Gamma = 1.0$, $M_1 = 1.0$, $M_2 = 1.0$, and $r_0 = 3$. The time interval used is $\Delta t = 1$, and lattice constant $\Delta x = \Delta y = 1$. In this paper, all variables are rescaled into dimensionless units.

3. Numerical results and discussion

First, we consider the late-stage snapshot of phase separation for the case of a pure asymmetric diblock copolymer without nanorods, as shown in Fig. 1(a). Herein, $f = 0.4$, phases A and B are represented by gray and white regions, respectively. The orientation of a hexagonally ordered cylinder is shown. This can be described as the "sea-island" structure, with the islands representing phase A and the sea



(a) (b)

Fig. 1. (a) Morphology for the self-assembly of pure asymmetric diblock copolymer without rods. Therein, $f = 0.4$, the gray regions are A domains, and the white regions are B domains. (b) Morphology for the self-assembly of pure rods with $L = 3$, $N = 240$, and $\chi = 0.5$.

representing phase B. Additionally, we simulate the self-assembly of pure nanorods in the absence of the diblock copolymer, as shown in Fig. 1(b). It is observed that the nanorods are uniformly dispersed in the lattice, forming an isotropic phase.

3.1. Phase diagram and nanostructures of diblock copolymer nanocomposite

When nanorods of different properties are placed in an asymmetrical diblock copolymer, the system self-assembles into different structures. Figure 2 shows the phase diagram of the polymer system with different numbers of rods (N) and different lengths of A-like sites (La). The number of nanorods N is varied from 10 to 300, the length of the nanorods L is 3, and the length of the A-like sites La is varied from 0 to 3. In the phase diagram, we find the various structures such as sea-island structure (SI), sea-island and lamellar structure (SI-L), and lamellar structure (L), and the representative structures are positioned on the right-hand side. The corresponding parameters of the SI are $N = 10$ and $La = 1$, those of SI-L are $N = 90$ and $La = 1$, and those of L are $N = 240$, $L = 1$, and $La = 2$.

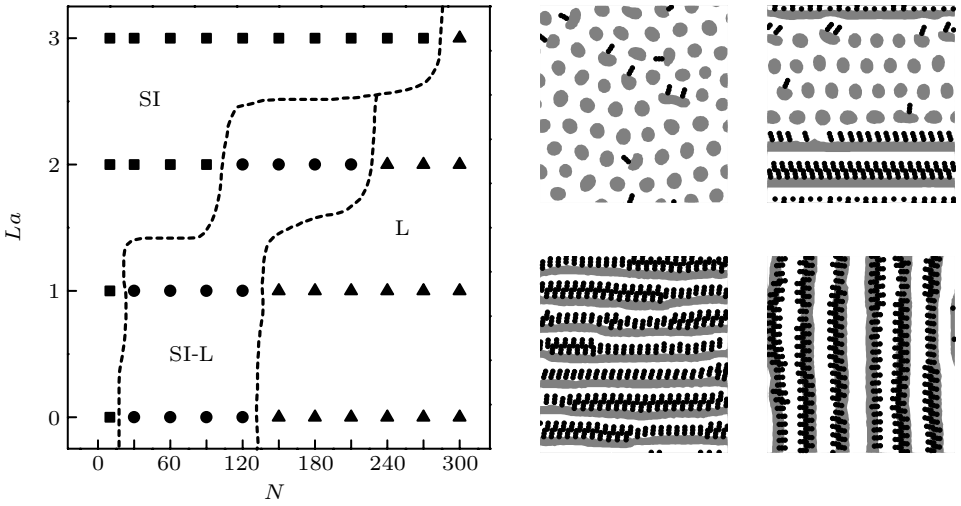


Fig. 2. Phase diagram of the asymmetrical diblock copolymer with different numbers of rods N and different lengths of A-like sites La. The dashed lines are used to distinguish the phase spaces of the different structures, which are abbreviated as SI (sea-island structure), SI-L (sea-island and lamellar structure), and L (lamellar structure). The morphologies on the right-hand side are the representative structures. Phases A and B are represented in gray and white, respectively.

When the numbers of nanorods are 10 and 300, the structures of the polymer system are unchanged with increasing La, being the sea-island and lamellar structures, respectively. However, the system undergoes phase transition from SI-L to SI with increasing La as the number of nanorods is varied from 30 to 120, and from L to SI as the number of nanorods is varied from 150 to 270. Interestingly enough, the disordered SI-L is in the state of two-phase coexistence, which are sea-island phase and lamellar phase, e.g., the representative structure on the right-hand side in Fig. 2. It is noteworthy that the lamellar structures are different when the number of nanorods is 240. We now focus on the case of $N = 240$. When $La = 0$, i.e., the nanorods are fully selective to the major phase (B), the asymmetrical diblock copolymer forms a tilted lamellar structure, with the nanorods forming a multilayer nanowire structure parallel to the phase interface between A and B. As the length of the A-like sites increases, the single-wetting nanorods transform into amphophilic nanorods and the system transforms into a parallel lamellar structure when $La = 1$, and subsequently into a perpendicular lamellar structure when $La = 2$. When the nanorods are fully selective to the minor phase (A), i.e., the amphophilic nanorods transform to single-wetting nanorods, the system exhibits a sea-island structure, in which the minor phase A is the island, and the major phase B is the sea.

The phenomena occurring in the parallel and perpendicular lamellar structure when $N = 240$, $La = 1$ and 2, respectively, and the SI-L when $N = 90$, $La = 1$, can be interpreted as follows: when the amphophilic rods are dispersed in the asymmetric diblock copolymer, most rods are pinned at the phase interface between A and B owing to the strong enthalpic effect. The rods with the same wettability show a trend of aggregation; however, this is suppressed by the phase interface and the rod-rod repulsive interaction. The competition of these interactions induces the nanorods to exhibit a side-to-side alignment almost perpendicular to the phase interface. At this point, the number of rods is 240, and the effect of the nanorods is significant. The side-to-side alignment results in a reduced interfacial energy in the system and promotes the stretching of polymer chains along the long axis of the rods. This results in the formation of a lamellar structure in the system. Meanwhile, the phase interface suppresses the movement of the rods; in turn, the rods suppress the motion of the polymer chains, thereby decreasing the conformational entropy of

the polymer. The loss of entropy contributes significantly to driving the phase AB to form a lamellar structure. Like the lamellar structure of $N = 240$, $La = 1$, the SI-L is also the result of the induce of nanorods. The same is the side-to-side alignment of most of the nanorods, it suppresses the movement of the polymer chain, and the conformation entropy of the polymer decreases. The loss of entropy plays an important role in driving partial AB phase to form a lamellar phase. In other words, the presence of nanorods makes the asymmetrical block copolymer with dispersed sea-island structure become continuous. However, compared with lamellar phase of $N = 240$, $La = 1$, the number of nanorods is relatively small, thus, the decreasing degree of entropy is not sufficient for the entire AB phase to form a lamellar phase. Therefore, the rest of AB phase forms a sea-island phase. Thus, the system is in the state of the two-phase coexistence when $N = 90$, $La = 1$. Meanwhile, most of the rods concentrate on the phase interface of lamellar phase, a few nanorods anchor at the phase interface of sea-island phase, leaving other areas rod-free.

Additionally, the polymer system transforms from SI to L with an increase in rod number, regardless of whether the nanorods are single-wetting ($La = 3$, $La = 0$) or amphophilic ($La = 1$, $La = 2$). Overall, the SI structures mainly concentrate in the regions of smaller N and larger La, as can be seen in the upper left of Fig. 2, and the L structures mainly concentrate in the regions of larger N and smaller La, as in the lower right of Fig. 2. Moreover, transformation to a lamellar structure is easier with an increase in rod number when the length of A-like sites is smaller. The number of rods that transformed to L becomes larger with increasing La.

In other words, compared with the nanorods that wetted the minor phase A, the nanorods that wetted the major phase B easily cause the system to form a lamellar structure. This is mainly because the diblock copolymer is asymmetric and forms a hexagonally cylindrical sea-island structure in the absence of nanorods. When the nanorods are placed in an asymmetric diblock copolymer, they can elongate the phase-A cylinder when $La = 3$. The greater the number of rods, the higher the number of elongated cylinders. When more elongated cylinders combine, the system forms a layered structure. However, when the nanorods are preferentially in phase B, the connecting structure (the sea) can easily form a link induced by nanorods and, hence, a layered structure. Therefore, when the rod number increases to 150, a layered structure is formed.

In terms of entropy, the polymer chain must be stretched because it is adsorbed on the surfaces of the nanorods; therefore, a decrease in the conformational entropy results in stretching of the polymer chain and formation of a layered structure. In terms of enthalpy, the formation of a lamellar structure is due to the interaction between the nanorods and polymer chains.

To further verify the phenomenon in which the system undergoes a transition from tilted lamellar to parallel lamellar, perpendicular lamellar, and then sea-island structure when $N = 240$, we numerically calculate the domain size $R_i(t)$, where $i = x$ or y in the x or y direction as a function of time. The domain size $R_i(t)$ can be derived from the inverse of the first moment of the structure $S(\boldsymbol{k},t)$ as $R_i(t) = 2\pi/\langle k_i(t)\rangle$, where $\langle k_i(t)\rangle = \int \mathrm{d}\boldsymbol{k} k_i S(\boldsymbol{k},t)/\int \mathrm{d}\boldsymbol{k} S(\boldsymbol{k},t)$. In fact, the structure factor $S(\boldsymbol{k},t)$ is determined by the Fourier component of the spatial concentration distribution.[64–66]

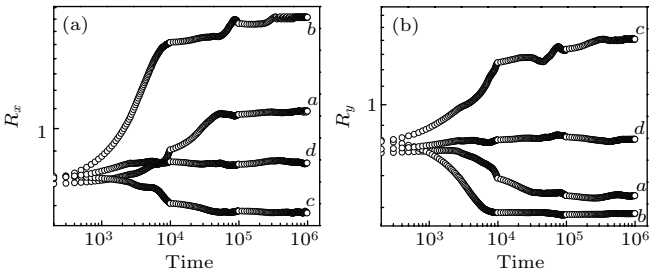


Fig. 3. Characteristic sizes of microdomains $R_x(t)$, $R_y(t)$ as a function of time in double logarithmic plots for different lengths of A-like sites when $N = 240$.

Figure 3 shows the double logarithmic plots of the microdomain size $R_i(t)$ in the x and y directions as a function of time. All the results are averaged over ten independent runs. Figure 3(a) shows the domain size $R_x(t)$ for different lengths of the A-like sites. At equilibrium, the domain size $R_x(t)$ initially increases (from curve a to curve b) with increasing length of the A-like sites, but then decreases significantly (from curve b to curve c) as the length of the A-like sites continues to increase. However, it increases again slightly (from curve c to curve d) as the length of the A-like sites approaches the maximum. This indicates that as the length of the A-like sites increases, coarsening of the domain occurs along the x-axis, corresponding to the parallel lamellar structure. Subsequently, the degree of coarsening is suppressed along the x-axis as the length of the A-like sites increases continually, corresponding to the perpendicular lamellar structure. However, with La increasing continually, $R_x(t)$ increases, corresponding to the sea-island structure.

By contrast, as shown in Fig. 3(b), the domain size $R_y(t)$ initially decreases (from curve a to curve b) and then increases (from curve b to curve c) before finally decreasing (from c to curve d) with increasing length of the A-like sites. This indicates that as the length of the A-like sites increases, coarsening of the microdomain in the y-axis is initially suppressed before being strengthened significantly. However, when the length of the A-like sites increases to the maximum, the coarsening of the microdomain is weakened. As shown in Fig. 3, the structures of the microdomains are stable as the domain size do not change with time at the later stage.

To monitor the process of ordered parallel and perpendicular lamellar structure formation discussed above, we show the

pattern evolution of asymmetric diblock copolymer/nanorods for $La = 1$ and $N = 240$ in Fig. 4, for $La = 2$ and $N = 240$ in Fig. 5, and the domain size on the x and y axes in Fig. 6.

Regarding the parallel lamellae, at the early stage ($t = 1 \times 10^3$) the asymmetric diblock copolymer exhibits a disordered structure, and the nanorods are pinned at the phase interface (Fig. 4(a)). Correspondingly, the domain size R_x is similar to R_y (Fig. 6(a)). When $1 \times 10^3 < t < 1 \times 10^5$, the domain tends to stretch along the x-axis, and the rods gradually accumulate into a side-to-side arrangement (Figs. 4(b)–4(d)). Meanwhile, the growth speed of the domain size R_x is much higher than that of R_y, as shown in Fig. 6(a). Subsequently, all the rods form a side-to-side arrangement and become almost perpendicular to the phase interface with time evolution (Figs. 4(e)–4(f)). Hence, the polymer system forms a parallel lamellar structure induced by the nanorods, and the domain size at equilibrium is $R_x \gg R_y$ (Fig. 6(a)).

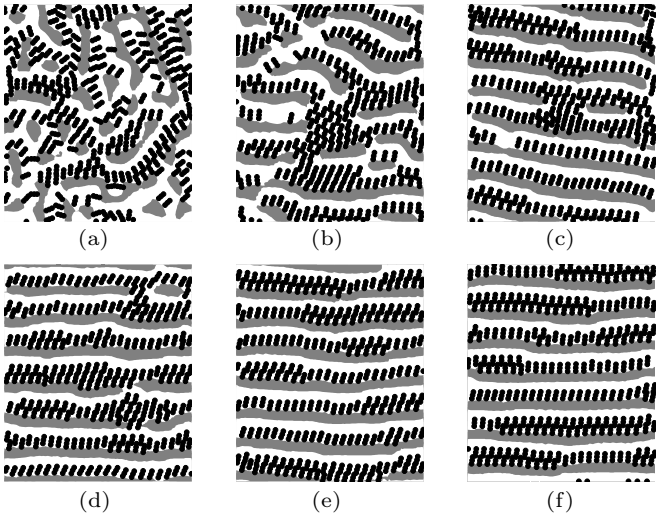


Fig. 4. Pattern evolution of asymmetric diblock copolymer/nanorods at different times corresponding to the parallel lamellae in Fig. 2. (a) $t = 1 \times 10^3$, (b) $t = 5 \times 10^3$, (c) $t = 1 \times 10^4$, (d) $t = 1 \times 10^5$, (e) $t = 5 \times 10^5$, (f) $t = 1 \times 10^6$. Phases A and B are represented by the colors of gray and white, respectively.

However, for the perpendicular lamellae, at an early stage ($t = 1 \times 10^3$), the polymer system tends to transform into a perpendicular lamellar structure (Fig. 5(a)). This indicates that the domain size R_y is slightly larger than R_x in the early stage (Fig. 6(b)). Similarly, the polymer system gradually forms an ordered perpendicular lamellar structure with time evolution, and the nanorods are vertically pinned at the phase interface (Figs. 5(b)–5(f)). Moreover, the domain size along the y-axis increases gradually, and that along the x-axis decreases gradually until it reaches a certain value, and $R_y \gg R_x$ (Fig. 6(b)). In addition, it is observed that the microdomain begins to grow slowly after a short time (i.e., $t > 100$). In the middle stage, the change in the microdomain size is obvious, but it stabilizes at the later stage. The microdomain size do not change for a long time, indicating that the obtained parallel and perpendicular lamellar structures are very stable.

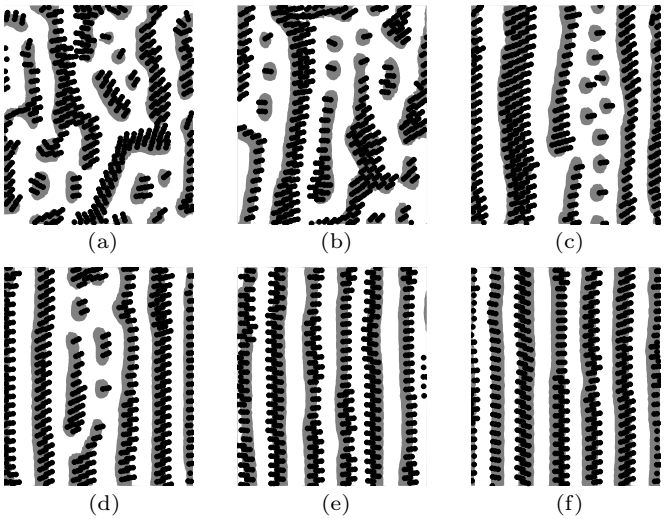


Fig. 5. Pattern evolution of asymmetric diblock copolymer/nanorods at different times corresponding to perpendicular lamellae in Fig. 2: (a) $t = 1 \times 10^3$, (b) $t = 5 \times 10^3$, (c) $t = 1 \times 10^4$, (d) $t = 1 \times 10^5$, (e) $t = 5 \times 10^5$, (f) $t = 1 \times 10^6$. Phases A and B are represented by the colors of gray and white, respectively.

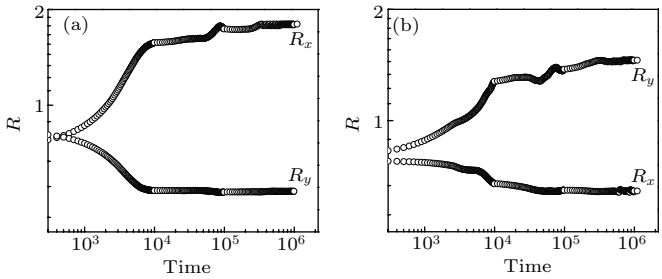


Fig. 6. Characteristic sizes of microdomains R_x, R_y as a function of time in double logarithmic plots corresponding to the parallel and perpendicular lamellae in Fig. 2: (a) $N = 240$, $La = 1$; (b) $N = 240$, $La = 2$.

3.2. Effect of other parameters on the diblock copolymer nanocomposite

One of the most promising research topics in nanotechnology is the preparation of high-order controllable nanostructures; hence, the formation of ordered lamellar structures doped with few A-like nanorods must be understood.

First, we vary the wetting strength for a rod number of 240 and investigate its effect on the phase behavior of asymmetric diblock copolymer/nanorods. Figure 7 demonstrates the self-assembly morphologies of asymmetric diblock copolymer/nanorods induced by different wetting strengths with $N = 240$. The results indicate that it forms an elongated sea (phase B)-island (phase A) structure, and the nanorods are pinned in the insular phase A (see Fig. 7(a)). As the wetting strength decreases, the polymer system tends to transform into a layered structure as shown in Fig. 7(b). When the wetting strength decreases to 0.04, the system completely transforms into a tilted layer as depicted by Fig. 7(c). The nanorods form a bilayer nanowire structure parallelled to the phase interface, and are all wetted in phase A. However, as the wetting strength

continues to decrease to 0.003, some nanorods escape from phase A, and the tilted layered structure has a few defects as shown in Fig. 7(d).

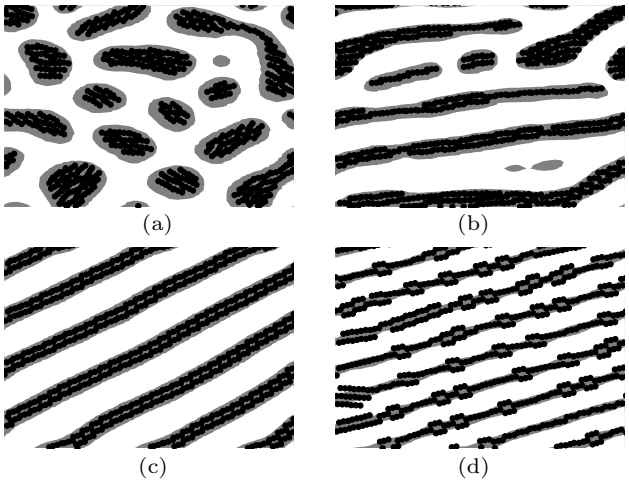


Fig. 7. Self-assembly morphologies of asymmetric diblock copolymer induced by nanorods of different wetting strengths, where $L = 3$, $La = 3$, $N = 240$, $\chi = 0.5$, and $\alpha = 0.02$: (a) $v_0 = 0.08$, (b) $v_0 = 0.05$, (c) $v_0 = 0.04$, (d) $v_0 = 0.003$. Phases A and B are represented by the colors of gray and white, respectively.

This is because the interaction between the nanorods and phase A decreases with decreasing wetting strength. Correspondingly, the contributions of free energy from the polymer and nanorods decreases, thereby decreasing the free energy of the system. An ordered tilted layered structure is formed when the wetting strength decreases. As the wetting strength decreases to 0.003, the interaction between the nanorods and phase A becomes sufficiently weak for nanorods to escape from phase A, and the structure shown in Fig. 7(d) is observed.

We vary the strength of long-range force of the asymmetric diblock copolymer to investigate its effect on the phase behavior of the asymmetric diblock copolymer/nanorods. When the number of nanorods is 240, the strength of the long-range force α increases gradually, as shown in Figs. 8(a)–8(d). The results show that when α is lower, the number of nanorods that aggregated in phase A is high (Fig. 8(a)). When the strength of the long-range force increases, phase A of the insular structure is elongated, as shown in Fig. 8(b). Subsequently, by continuously increasing α to 0.07, the elongated phase A regions connect partially, and the domain width decreases significantly. However, some phase-A regions are not stretched and form a tilted layered structure (Fig. 8(c)). As we continue increasing α to 0.11, all the elongated phase A regions connect, and the domain width decreases slightly compared with the width when α is 0.07. The polymer system forms a tilted lamellar structure with few defects. Some nanorods exhibit end-to-end arrangement parallelled to the phase interface, and the rest are arranged in a good order at an angle with the phase interface, as shown in Fig. 8(d).

It is well-known that the strength of the long-range force is inversely proportional to the polymerization degree and domain thickness; hence, the larger the parameter α, the smaller the polymerization degree and domain thickness.[67] When α is small, the polymerization degree and domain thickness are larger. This induces the nanorods aggregate in phase A, resulting in islands disperse into phase B. However, as α increases, the polymerization degree and domain thickness decrease, thereby elongating the phase-A regions; consequently, the aggregates interconnect and form a layered structure. Thus, it is easier to form a tilted lamellar structure when the polymerization degree is smaller.

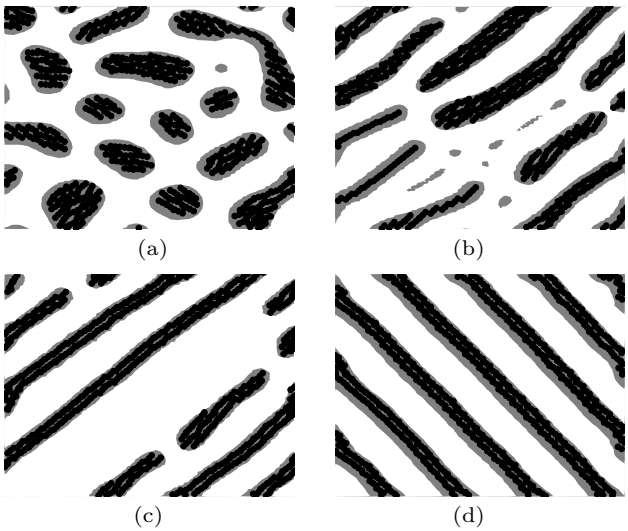


Fig. 8. Self-assembly morphologies of asymmetric diblock copolymer/nanorods induced by different strengths of the long-range force, where $L = 3$, $La = 3$, $v_0 = 0.08$, $\chi = 0.5$, and $N = 240$: (a) $\alpha = 0.02$, (b) $\alpha = 0.04$, (c) $\alpha = 0.07$, (d) $\alpha = 0.11$. Phases A and B are represented by the colors of gray and white, respectively.

Moreover, we vary the rod-rod interaction of single-wetting nanorods to investigate its effect on the self-assembly behavior of asymmetric diblock copolymer/nanorods, as shown in Fig. 9. The results show that the polymer system transforms from an elongated sea-island structure to a tilted lamellar structure as depicted by Figs. 9(a)–9(d). The arrangement of the nanorods differs from the previous tilted lamellar structure. Owing to the stronger rod-rod interaction, the nanorods are almost perpendicular to the phase interface.

Finally, we increase the length of the rods and investigate its effect on the phase behavior of the asymmetric diblock copolymer/nanorods, as shown in Fig. 10. The results show that the polymer system has a greater tendency to form lamellae with increasing rod length for a rod number of 240, as depicted in Figs. 10(a)–10(b). However, when we decrease the rod number to 190 for the length $L = 4$, the system transforms into a tilted lamellar structure (Fig. 10(c)). By continuously increasing the rod length up to 5, a tilted lamellar structure is observed for a rod number of 154 (Fig. 10(d)). In other words, the polymer system easily forms an ordered tilted lamellar structure when the number of nanorods is small and the length of the nanorods is greater.

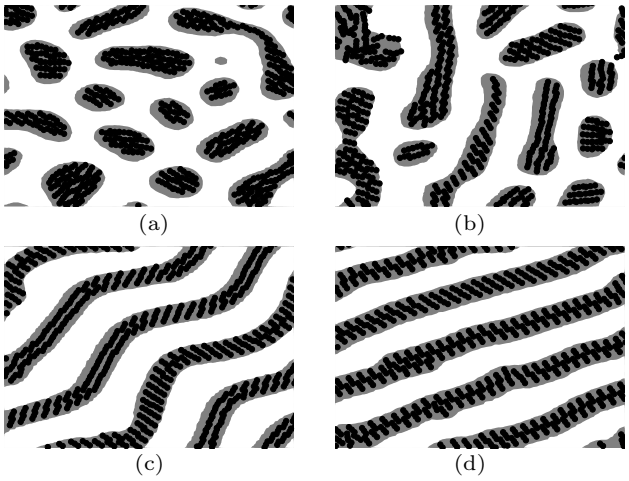


Fig. 9. Self-assembly morphologies of asymmetric diblock copolymer/nanorods induced by different amounts of rod-rod interaction, where $L = 3$, $La = 3$, $N = 240$, $v_0 = 0.08$, and $\alpha = 0.02$: (a) $\chi = 0.5$, (b) $\chi = 0.9$, (c) $\chi = 0.95$, (d) $\chi = 0.98$. Phases A and B are represented by the colors of gray and white, respectively.

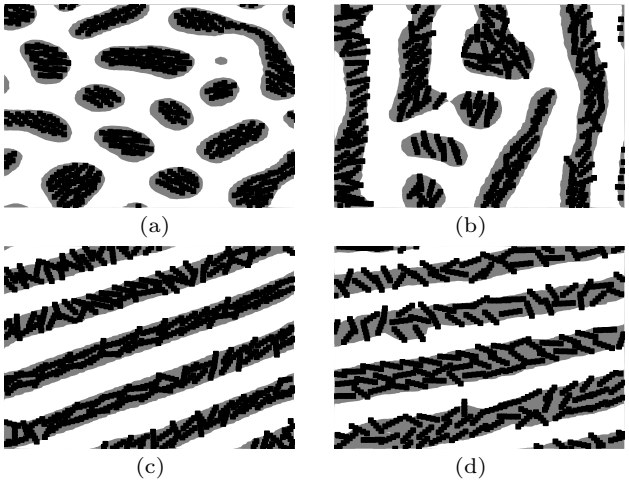


Fig. 10. Self-assembly morphologies of asymmetric diblock copolymer/nanorods induced by different rod lengths, where $v_0 = 0.08$, $\alpha = 0.02$, and $\chi = 0.5$: (a) $L = 3$, $La = 3$, $N = 240$; (b) $L = 4$, $La = 4$, $N = 240$; (c) $L = 4$, $La = 4$, $N = 190$; (d) $L = 5$, $La = 5$, $N = 154$. Phases A and B are represented by the colors of gray and white, respectively.

4. Conclusions

Based on cell dynamics simulation and Brown dynamics, we investigate the microphase transition of an asymmetric diblock copolymer induced by nanorods of different properties. The results show the phase diagram and representative nanostructures of the diblock copolymer nanocomposite. In the phase diagram, various structures such as SI, SI-L, and L can be observed. When the numbers of nanorods are 10 and 300, the structures of the polymer system are unchanged with increasing *La*, being the SI and L structures, respectively. However, the system undergoes phase transition from SI-L to SI with increasing *La* as the number of nanorods is varied from 30 to 120, and from L to SI as the number of nanorods is varied from 150 to 270. The system transforms from SI to L with increasing rod number regardless of whether the nanorods are single-wetting or amphophilic. However, it is easier to transform the system into a lamellar structure with the increasing rod number when the length of the A-like sites is smaller. It is worth mentioning that phase transition occurs from a tilted layered structure to a parallel lamellar, perpendicular lamellar, and subsequently the sea-island structure by increasing the length of A-like sites of the rod when the rod number is 240. For this transition, we further analyze the dynamic evolution of the domain size. Subsequently, we investigate the pattern evolution and domain growth of the ordered parallel and perpendicular lamellar structures. Furthermore, we investigate the effects of the wetting strength, polymerization degree, rod-rod interaction and length of the rods on the phase behaviors of the asymmetric diblock copolymer/nanorods. When the wetting strength and polymerization degree are smaller, and the rod-rod interaction and length of nanorods are greater, the polymer system easily forms an ordered tilted lamellar structure. Our simulations provide an efficient method of obtaining an ordered structure on the nanometer scale and designing functional materials with optical, electronic, and magnetic properties.

References

[1] Peng G W, Qiu F, Ginzburg V V, Jasnow D and Balazs A C 2000 *Science* **288** 1802
[2] Chen K and Ma Y Q 2002 *Phys. Rev. E* **65** 041501
[3] Chen K and Ma Y Q 2002 *J. Chem. Phys.* **116** 7783
[4] He L L, Zhang L X, Xia A and Liang H J 2009 *J. Chem. Phys.* **130** 144907
[5] He L L, Zhang L X, Chen H P and Liang H J 2009 *Polymer* **50** 3403
[6] He L L, Zhang L X and Liang H J 2010 *Polymer* **51** 3303
[7] Chakraborty S and Roy S 2015 *J. Phys. Chem. B* **119** 6803
[8] Zhou Y X, Huang M X, Lu T and Guo H X 2017 *Macromolecules* **51** 3135
[9] Tang Q Y and Ma Y Q 2009 *J. Phys. Chem. B* **113** 10117
[10] Yan L T and Balazs A C 2011 *J. Mater. Chem.* **21** 14178
[11] Yan L T, Maresov E, Buxton G A and Balazs A C 2011 *Soft Matter* **7** 595
[12] Zhang D, Cheng J, Jiang Y W, Wen X H and Zhang L X 2013 *J. Polym. Sci. Part B: Polym. Phys.* **51** 392
[13] Park J H and Joo Y L 2014 *Phys. Chem. Chem. Phys.* **16** 8865
[14] Gao Y Y, Liu J, Shen J X, Zhang L Q and Cao D P 2014 *Polymer* **55** 1273
[15] Chao H, Lindsay B J and Riggleman R A 2017 *J. Phys. Chem. B* **121** 11198
[16] Osipov M A, Ushakova A S and Gorkunov M V 2017 *Liq. Cryst.* **44** 1861
[17] Osipov M A, Kudryavtsev Y V, Ushakova A S and Berezkin A V 2018 *Liq. Cryst.* **45** 2065
[18] Karatrantos A, Composto R J, Winey K I and Clarke N 2019 *Macromolecules* **52** 2513
[19] He L L, Zhang R F and Ji Y Y 2012 *Chin. Phys. B* **21** 088301
[20] Wang X H, Li S B, Zhang L X and Liang H J 2011 *Chin. Phys. B* **20** 083601
[21] Zhang Q L, Gupta S, Emrick T and Russell T P 2006 *J. Am. Chem. Soc.* **128** 3898
[22] Ploshnik E, Salant A, Banin U and Shenhar R 2010 *Phys. Chem. Chem. Phys.* **12** 11885
[23] Deshmukh R D, Liu Y and Composto R J 2007 *Nano Lett.* **7** 3662
[24] Nepal D, Onses M S, Park K, Jespersen M, Thode C J, Nealey P F and Vaia R A 2012 *ACS Nano* **6** 5693
[25] Thorkelsson K, Mastroianni A J, Ercius P and Xu T 2012 *Nano Lett.* **12** 498
[26] Thorkelsson K, Nelson J H, Alivisatos A P and Xu T 2013 *Nano Lett.* **13** 4908
[27] Lai F Y, Tasciuc T B and Plawsky J 2015 *Nanotechnology* **26** 055301

[28] Krook N M, Ford J, Marechal M, Rannou P, Murray C B and Composto R J 2018 *ACS Macro. Lett.* **7** 1400

[29] Diaz J, Pinna M, Zvelindovsky A V, Pagonabarraga I and Shenhar R 2020 *Macromolecules* **53** 3234

[30] Krook N M, Tabedzki C, Elbert K C, Yager K G, Murray C B, Riggleman R A and Composto R J 2019 *Macromolecules* **52** 8989

[31] Rasin B, Lindsay B J, Ye X C, Mech J S, Riggleman R A and Composto R J 2020 *Soft Matter* **16** 3005

[32] Glor E C, Ferrier R C, Li C, Composto R J and Fakhraai Z 2017 *Soft Matter* **13** 2207

[33] Diaz J, Pinna M, Zvelindovsky A V and Pagonabarraga I 2019 *Macromolecules* **52** 8285

[34] Tao J, Lu Y H, Zheng R S, Lin K Q, Xie Z G, Luo Z F, Li S L, Wang P and Ming H 2008 *Chin. Phys. Lett.* **25** 4459

[35] Walther A, Drechsler M, Rosenfeldt S, Harnau L, Ballauff M, Abetz V and Müller A H E 2009 *J. Am. Chem. Soc.* **131** 4720

[36] Ruhland T M, Gröschel A H, Walther A and Müller A H E 2011 *Langmuir* **27** 9807

[37] Xu K, Guo R H, Dong B J and Yan L T 2012 *Soft Matter* **8** 9581

[38] Tripathy M and Schweizer K S 2013 *J. Phys. Chem. B* **117** 373

[39] Kharazmi A and Priezjev N V 2017 *J. Phys. Chem. B* **121** 7133

[40] Guo Y Q, Pan J X, Sun M N and Zhang J J 2017 *J. Chem. Phys.* **146** 024902

[41] Ginzburg V V, Qiu F, Paniconi M, Peng G W, Jasnow D and Balazs A C 1999 *Phys. Rev. Lett.* **82** 4026

[42] Qiu F, Ginzburg V V, Paniconi M, Peng G W, Jasnow D and Balazs A C 1999 *Langmuir* **15** 4952

[43] Buxton G A and Balazs A C 2004 *Mol. Simulat.* **30** 249

[44] Balazs A C, Ginzburg V V, Qiu F, Peng G W and Jasnow D 2000 *J. Phys. Chem. B* **104** 3411

[45] Geng X B, Pan J X, Zhang J X, Sun M N and Cen J Y 2018 *Chin. Phys. B* **27** 058102

[46] Cahn J W and Hilliard J E 1958 *J. Chem. Phys.* **28** 258

[47] Cahn J W 1959 *J. Chem. Phys.* **30** 1121

[48] Cahn J W 1961 *Acta Metall.* **9** 795

[49] Cahn J W and Hilliard J E 1971 *Acta Metall.* **19** 151

[50] Glotzer S C and Coniglio A 1994 *Phys. Rev. E* **50** 4241

[51] Glotzer S C, StauKer D and Jan N 1994 *Phys. Rev. Lett.* **72** 4109

[52] Glotzer S C, Di Marzio E A and Muthukumar M 1994 *Il Nuovo Cimento* **16** 1171

[53] Glotzer S C, Di Marzio E A and Muthukumar M 1995 *Phys. Rev. Lett.* **74** 2034

[54] Puri S and Frisch H L 1994 *J. Phys. A: Math. Gen.* **27** 6027

[55] Puri S and Frisch H L 1998 *Int. J. Mod. Phys. B* **12** 1623

[56] Zhang L C, Sun M N, Pan J X, Wang B F, Zhang J J and Wu H S 2013 *Chin. Phys. B* **22** 096401

[57] Pan J X, Zhang J J, Wang B F, Wu H S and Sun M N 2013 *Chin. Phys. B* **22** 026401

[58] Pan J X, Zhang J J, Wang B F, Wu H S and Sun M N 2013 *Chin. Phys. Lett.* **30** 046401

[59] Guo Y Q, Pan J X, Zhang J J, Sun M N, Wang B F and Wu H S 2016 *Acta Phys. Sin.* **65** 056401 (in Chinese)

[60] Oono Y and Bahiana M 1988 *Phys. Rev. Lett.* **61** 1109

[61] Bates F S and Fredrickson G H 1990 *Annu. Rev. Phys. Chem.* **41** 525

[62] Chakrabarti A and Gunton J D 1993 *Phys. Rev. E* **47** R792

[63] Oono Y and Puri S 1987 *Phys. Rev. Lett.* **58** 836

[64] Oono Y and Puri S 1988 *Phys. Rev. A* **38** 434

[65] Shinozaki A and Oono Y 1992 *Phys. Rev. A* **45** R2161

[66] Shinozaki A and Oono Y 1993 *Phys. Rev. E* **48** 2622

[67] Ohta T and Kawasaki K 1986 *Macromolecules* **19** 2621